

# Large Magnetoelectric Coupling in the Thin Film of Multiferroic CuO

Sudipta Goswami,\* Koushik Dey, Supriyo Chakraborty, Saurav Giri, Ujjal Chowdhury, and Dipten Bhattacharya



Cite This: <https://dx.doi.org/10.1021/acsomega.0c02211>



Read Online

ACCESS |



Metrics & More

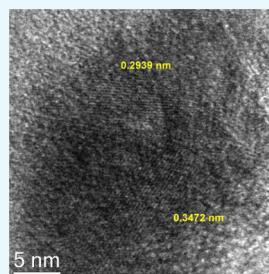


Article Recommendations

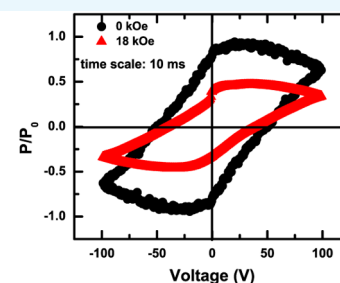


Supporting Information

**ABSTRACT:** We report observation of large magnetoelectric coupling in an epitaxial thin film of multiferroic CuO grown on the (100)MgO substrate by the pulsed laser deposition technique. The film is characterized by X-ray diffraction, transmission electron microscopy, and Raman spectrometry. The crystallographic structure of the film turns out to be monoclinic (space group  $C2/c$ ) with  $[111]\text{CuO}||[100]\text{MgO}$  “out-of-plane” epitaxy and “in-plane” domain structure. The lattice misfit strain is found to vary within  $\pm 1\text{--}3\%$ . The dc resistivity, magnetization, dielectric spectroscopy, and remanent ferroelectric polarization have been measured across 80–300 K. The dielectric constant is found to decrease by  $>20\%$  under a moderate magnetic field of  $\sim 18$  kOe while the remanent ferroelectric polarization, emerging at the onset of magnetic transition ( $T_N \sim 175$  K), decreases by nearly 50% under  $\sim 18$  kOe field. These results could assume importance as the strain-free bulk CuO does not exhibit magnetoelectric coupling within such magnetic field regime. The strain-induced large magnetoelectric coupling in the CuO thin film would generate new possibility of further strain tuning to observe room-temperature magnetoelectric multiferroicity suitable for scores of applications such as memories, sensors, energy-harvesting devices, generators, amplifiers, and so forth.



(a)



(b)

## 1. INTRODUCTION

The magnetoelectric multiferroic systems, exhibiting coexisting ferroelectric and magnetic orders as well as a cross-coupling between the respective order parameters, are extremely attractive for a variety of future generation spintronics-based applications.<sup>1,2</sup> They range from four-state memories, sensors, spin-wave amplifiers, or magnetoelectric generators to biomedical implants capable of correcting the gating action in damaged ion channels. However, for most of the applications as spintronic devices, large magnetoelectric coupling is desirable at room temperature. Quite naturally,  $\text{BiFeO}_3$  has generated maximum interest because of its room-temperature multiferroicity.<sup>3</sup> Even then, large leakage current, volatility of Bi, and consequent formation of secondary phases during its synthesis, weak magnetoelectric coupling under moderate magnetic or electric field raise doubts about its large scale practical usage. Alternative candidate systems such as  $\text{Bi}_5\text{Ti}_3\text{Fe}_{0.7}\text{Mn}_{0.3}\text{O}_{15}$ ,  $\text{Bi}_5\text{Ti}_3\text{Fe}_{0.7}\text{Co}_{0.3}\text{O}_{15}$ ,  $\text{Sr}_3\text{Co}_2\text{F}_{24}\text{O}_{41}$ , and so forth have indeed been discovered<sup>4</sup> during this period of renaissance in single-phase multiferroic systems since 2000. Ideally, a type-II multiferroic, where magnetism drives onset of ferroelectricity at or above room temperature, is the most suitable candidate.<sup>5</sup> This is because the change in the magnetic structure and/or anisotropy under externally applied magnetic field gives rise to enormous change in the ferroelectric polarization in such systems. Recent work<sup>6–9</sup> on CuO (tenorite) should have generated considerable interest, in

this context, because of its type-II multiferroicity at close to room temperature ( $\sim 230$  K). The incommensurate spiral magnetic structure breaks the inversion symmetry and drives onset of ferroelectricity at the magnetic transition temperature  $T_N$  ( $\sim 230$  K). From density functional theory and Monte-Carlo simulation, it has been shown that, under 20–40 GPa pressure, increase in the magnetic exchange coupling results in shifting of the  $T_N$  toward room temperature with more than three-fold increase in polarization.<sup>10</sup> Limited experimental support for pressure-driven room-temperature multiferroicity has also been received,<sup>11</sup> which, of course, was challenged subsequently.<sup>12</sup> However, in spite of coexistence of ferroelectric and magnetic orders, the magnetoelectric coupling turns out to be poor<sup>13</sup> except at an extremely high field regime ( $\sim 500$  kOe) [ref 14]. This seems to have prevented generation of widespread interest in the multiferroicity of CuO. In this paper, we show, for the first time, that in a thin film of CuO, grown epitaxially on the (100)MgO substrate with  $[111]$ -axis perpendicular to the film surface, the magnetodielectric effect is substantial ( $>20\%$ ) even under a magnetic field of  $\sim 18$  kOe.

Received: May 12, 2020

Accepted: August 20, 2020



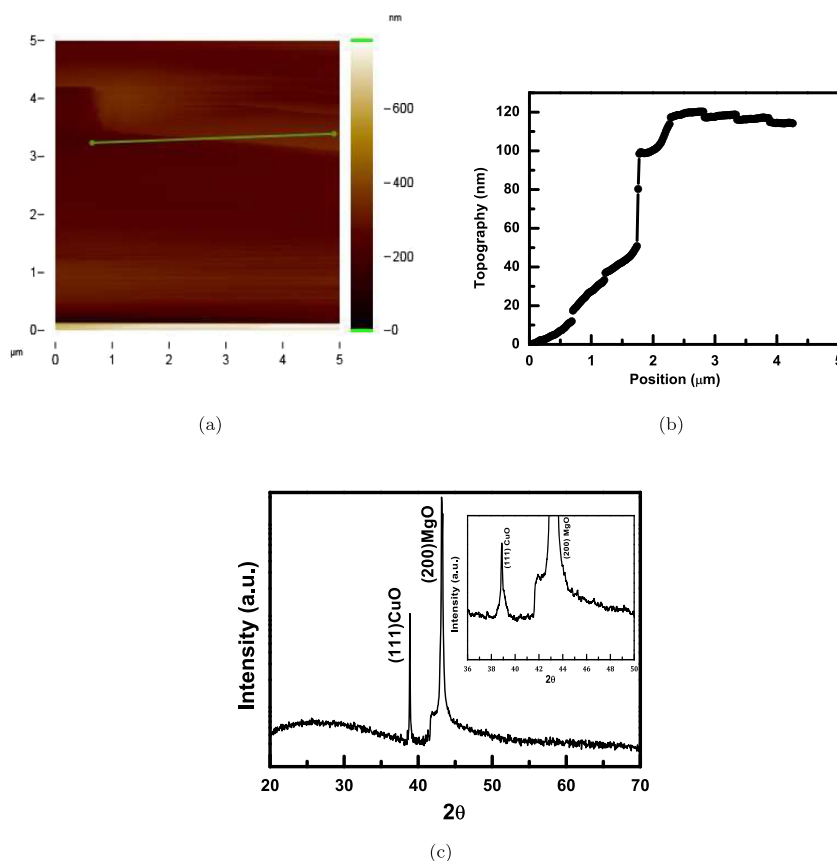


**Figure 1.** Representative (a) AFM topography image and (b) the line profile across the line shown in (a); (c) XRD  $\theta$ - $2\theta$  scan at room temperature across  $20$ – $70^\circ$ ; only (111) and (200) peaks could be observed from the film and substrate, respectively; no additional phase is present; the inset shows the blown-up peaks.

Finite remanent ferroelectric polarization is also found to emerge at  $T_N$ , which undergoes suppression by  $\sim 50\%$  under  $\sim 18$  kOe signifying the presence of strong magnetoelectric coupling.

## 2. RESULTS AND DISCUSSION

Figure 1a shows the representative atomic force microscopy (AFM) image recorded across a scratch, which exposes the film/substrate interface. The line profile across the scratch (Figure 1b) reveals the film thickness to be  $\sim 100$  nm. The average surface roughness of the film is found to be  $\sim 10$  nm. An additional line profile image and data collected across other parts of the film are shown in the Supporting Information. Figure 1c shows the result of  $\theta$ - $2\theta$  X-ray diffraction (XRD) scan recorded across a  $2\theta$  range ( $20$ – $70^\circ$ ). The (111) peak of CuO at  $2\theta = 38.8^\circ$  (JCPDS file 05-0661) could be observed close to the (200) peak of MgO signifying a high degree of out-of-plane epitaxy with  $[111]\text{CuO}||[100]\text{MgO}$ .<sup>15–18</sup> The low-angle shoulder around the (200) peak of MgO possibly results from oscillation in the diffraction intensity because of the Laue function term. The presence of peaks from other crystallographic planes could not be observed within this  $2\theta$  range. Also, no peak from the  $\text{Cu}_2\text{O}$  phase could be seen. Interestingly, although out-of-plane epitaxy (or, at least, a large scale texturing) is found to be present, in-plane epitaxy is lost. This has been observed by others as well for CuO thin films deposited on the (100)MgO substrate by both pulsed laser deposition and molecular beam epitaxy.<sup>15–18</sup> For instance, Catana et al.<sup>16</sup> shown from cross-sectional transmission

electron microscopy (TEM) that for films grown by pulsed laser deposition technique, the in-plane epitaxy is maintained only locally with three major epitaxial relationships  $[\bar{1}10]\text{CuO}||[110]\text{MgO}$ ,  $[0\bar{1}1]\text{CuO}||[110]\text{MgO}$ , and  $[10\bar{1}]\text{CuO}||[100]\text{MgO}$ . Similarly, molecular beam epitaxy technique too produces a film with out-of-plane  $[111]\text{CuO}||[100]\text{MgO}$  epitaxy yet in-plane polycrystallinity.<sup>15,18</sup> In the present case, we have used high-resolution TEM (HRTEM) rigorously to examine the in-plane crystallographic orientation of the film by capturing images from different edges of the film—primarily parallel to the film surface and away from the film/substrate interface. Figure 2a,d shows two representative HRTEM micrographs. More such images are available in the Supporting Information document. For more accurate determination of  $d$ -spacings of the lattice planes, first Fourier transformation (FFT) of the raw HRTEM image was generated, which was then inverted to yield clearer images of the lattice fringes. For instance, Figure 2b is the FFT of the selected region of Figure 2a. It shows two pairs of spots for two different planes, (112) and (112). Figure 2c shows the corresponding lattice planes (generated from inverse FFT of Figure 2b), where (112) with  $d_{hkl} = 1.9590$  Å, and (112) with  $d_{hkl} = 1.7780$  Å. Similarly, selection from Figure 2d provides characteristic FFT [Figure 2e] with spots for (112) and (202). Figure 2f shows the corresponding lattice planes, simulated (inverse FFT) from Figure 2e, where (112) with  $d_{hkl} = 1.7780$  Å and (202) with  $d_{hkl} = 1.8660$  Å. The presence of strain is clear, as shown in Figure 2d, as complex orientation is seen at regions where two (multiple) participating planes coexist at different orientations.

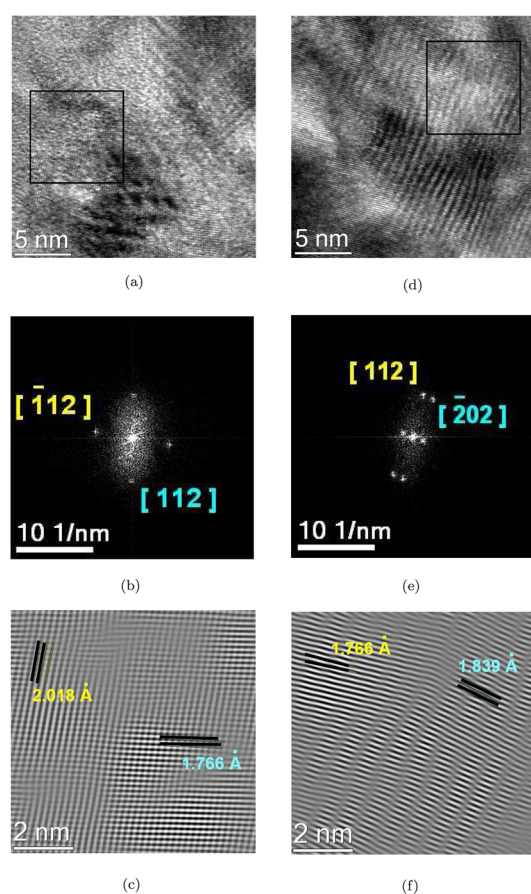


**Figure 2.** (a,d) High-resolution transmission electron microscopic images of the CuO film; (b,e) are the FFT of the selected areas marked in (a,d); and (c,f) are the corresponding simulated lattice planes from the FFTs of (a,d).

Using the lattice fringes observed in HRTEM and the reflection in XRD, the lattice parameters for the thin film were obtained. The bulk CuO is found to assume the monoclinic  $C2/c$  structure at room temperature<sup>6</sup> with lattice parameters  $a = 4.68 \text{ \AA}$ ,  $b = 3.42 \text{ \AA}$ ,  $c = 5.129 \text{ \AA}$ , and  $\beta = 99.54^\circ$ . Interestingly, as found out from the analysis of HRTEM data, the thin film too, grown on cubic (100)MgO, exhibits the monoclinic  $C2/c$  lattice. This has been observed by others as well.<sup>15–18</sup> In the present case, the lattice parameters are estimated to be  $a = 4.337 \text{ \AA}$ ,  $b = 3.666 \text{ \AA}$ ,  $c = 5.218 \text{ \AA}$ , and  $\beta = 101.75^\circ$ . The in- and out-of-plane strains have also been estimated. The out-of-plane compressive strain is found out to be  $\sim 0.4\%$  while the in-plane domains contain both compressive and tensile strains varying within  $\sim 1\text{--}3\%$ . Detailed investigation of different regions of the film by HRTEM shows the formation of domains of size varying within 10–20 nm (Supporting Information). This result is consistent with the domain size ( $\sim 40 \text{ nm}$ ) obtained from Debye–Scherrer analysis of the XRD peak. The presence of tensile strain in some regions while compressive in the other gives rise to the formation of finer domains. It is important to discuss here the reason behind the loss of in-plane epitaxy in the present case. It is actually because of large difference between the symmetry and crystallographic structure of CuO and MgO. The monoclinic CuO has been grown epitaxially on cubic MgO. Similar “lattice-mismatched epitaxial growth” could be observed in other systems as well.<sup>19</sup> Because the

(111) plane of CuO is closely matched with the (100) plane of MgO, out-of-plane epitaxy could be observed. However, in the in-plane region, small to large lattice mismatch could be observed between crystallographic planes of CuO and those of MgO; smaller mismatch leads to smaller strain and epitaxial growth whereas larger strain gives rise to loss of epitaxy within a few layers. In fact, the critical thickness at which epitaxy is lost varies inversely with the lattice mismatch. For minimization of free energy, this leads to formation of domains with defects at domain boundaries beyond the critical thickness as observed by us as well as by Catana et al.<sup>16</sup> The analysis of the cross-sectional TEM data<sup>16</sup> further points out that lattice mismatch or epitaxial strain varies from  $\sim 1\%$  in the case of  $[\bar{1}10]\text{CuO}||[110]\text{MgO}$  to  $\sim 10\%$  for  $[10\bar{1}]\text{CuO}||[100]\text{MgO}$ . By considering the interaction potential between atoms of the overlay, substrate, and interface region, it has been shown theoretically also<sup>16</sup> that such epitaxial relationship minimizes the interface energy. Therefore, in the present case too, same epitaxial relationship is expected to prevail. We now address the issue of chemical strain as a result of off-stoichiometry. Experimentally as well as from thermodynamic calculations,<sup>20</sup> it has been shown that two stable oxides—CuO and  $\text{Cu}_2\text{O}$ —could form. Higher temperature ( $>600^\circ\text{C}$ ) and low oxygen pressure are expected to yield the  $\text{Cu}_2\text{O}$  phase. This has been observed by others also.<sup>15,18,21–23</sup> In the present case, appropriate substrate temperature, background oxygen pressure, and postannealing treatment under oxygen (discussed in the Experimental Section) have been maintained to ensure formation of stoichiometric CuO. Like others,<sup>15,18,21–23</sup> the XRD data (Figure 1c) do not show the presence of  $\text{Cu}_2\text{O}$  phase. In all these cases, chemical analysis (by redox titration) also does not show the presence of significant off-stoichiometry. Therefore, the role of chemical strain turns out to be insignificant in the present case, and magnetoelectric properties are, primarily, governed by epitaxial strain. The Supporting Information includes the Raman spectra for the film and the substrate recorded at room temperature (Figure S1). With respect to the observations made in strain-relaxed bulk single crystal of CuO, the Raman peaks exhibit shift as well as much larger full-width at half maximum (fwhm). For instance, although for single crystal, the fwhm of the peaks varies within  $\sim 6$  to  $\sim 8 \text{ cm}^{-1}$  [ref 24], and the corresponding data for the thin film are  $\sim 13$  to  $\sim 19 \text{ cm}^{-1}$ . Large fwhm signifies the presence of strain-driven disorder. The Raman mode shift of  $\sim 2.5 \text{ cm}^{-1}$  is used to determine the film thickness from the relationship among stress in the film, film thickness, and Raman mode shift.<sup>25,26</sup> The film thickness turns out to be  $\sim 100 \text{ nm}$ , which corroborates the result obtained from direct measurement by AFM. From the XRD, HRTEM, and Raman spectrometry experiments, it appears that the CuO film exhibits out-of-plane epitaxy (or, at least, large scale texturing) but the in-plane epitaxy is lost. Instead, finer domains of size  $\sim 10\text{--}20 \text{ nm}$  form as a result of large lattice misfit strain. Influence of the strain driven disorder is reflected in the electrical and magnetic properties. The dielectric permittivity exhibits a frequency-dependent shift of the anomaly around  $T_N$  while analysis of the magnetization data shows an order of magnitude large Weiss constant ( $\theta$ ). However, alongside inducing formation of finer in-plane domains, the lattice misfit strain in the film appears to play a significant role in yielding large magnetoelectric coupling under a rather moderate magnetic field.

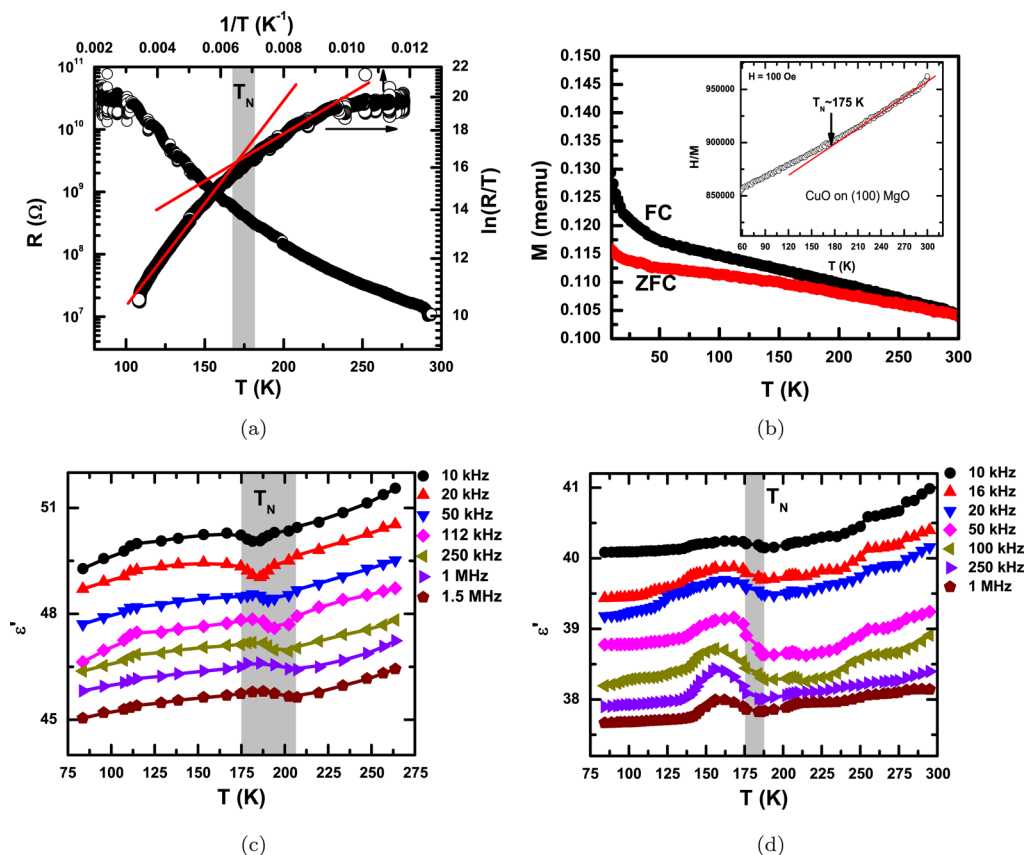
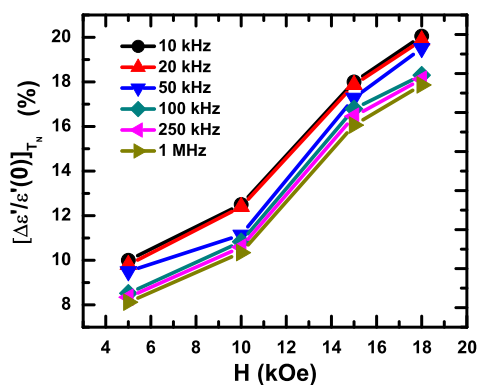


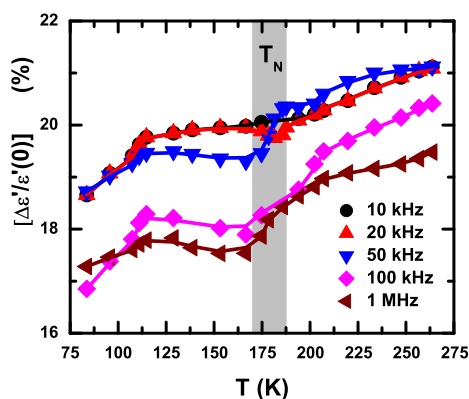
**Figure 3.** (a) dc resistance ( $R$ ) vs temperature ( $T$ ) and  $\ln(R/T)$  vs  $1/T$  plots, (b) ZFC and FC magnetization vs temperature data obtained under the 100 Oe field; the inset shows the fitting with the Curie–Weiss law;  $T_N$  turns out to be  $\sim 175$  K; (c,d) real parts of the dielectric permittivity as a function of temperature at different frequencies within 10 kHz to 2 MHz under zero and  $\sim 18$  kOe magnetic field.

We now turn our attention to the electrical and magnetic properties of the film. Figure 3 summarizes the main results of the paper. Figure 3a shows the dc resistance ( $R$ ) versus temperature ( $T$ ) and  $\ln(R/T)$  versus  $1/T$  plots. The zero-field-cooled (ZFC) and field-cooled (FC) magnetization ( $M$ ) versus  $T$  plots are shown in Figure 3b. The Curie–Weiss analysis of the ZFC magnetization versus temperature data (Figure 3b inset) yields the magnetic transition temperature ( $T_N$ ) to be  $\sim 175$  K in the thin film. The  $\ln(R/T)$  versus  $1/T$  plot too depicts clear change in the slope at  $T_N$  signifying change in the activation energy of the hopping conduction at below and above  $T_N$  (Figure 3a). Interestingly, from the Curie–Weiss analysis of the magnetization data, the Weiss constant  $\theta$  turns out to be  $\sim 1715$  K signifying large  $\theta/T_N$  ( $\sim 9.8$ ) as a result of strain-driven disorder. It is also important to mention that the divergence between ZFC and FC magnetization data starts at  $\sim 230$  K, which is above the  $T_N$  obtained from Curie–Weiss fitting. This is also a reflection of the presence of short-range order within an otherwise paramagnetic matrix. Figure 3c,d shows the real parts of the dielectric permittivity ( $\epsilon'$ ) as a function of temperature under zero and  $\sim 18$  kOe field, respectively, at several frequencies within 10 kHz to 2 MHz. The imaginary parts ( $\epsilon''$ ), on the other hand, are shown in the Supporting Information (Figures S5 and S6). We have determined this frequency range to be corresponding to the relaxation of the intrinsic capacitive response of the sample from the analysis of complex-plane impedance spectra. The dielectric anomaly around  $T_N$  exhibits frequency-dependent shift toward higher temperature as commonly observed in

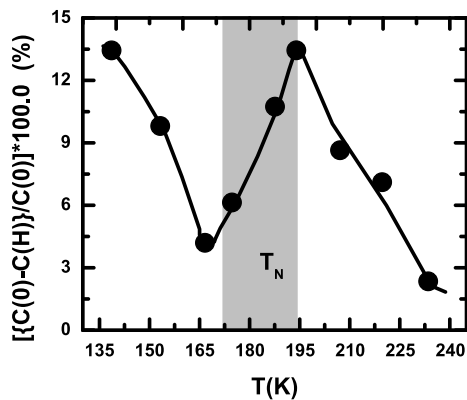
relaxor systems or in systems containing disorder. The nature of the anomaly—a broad peak followed by a dip and, then, a rise as the temperature is further increased above  $T_N$ —also signifies the presence of disorder vis-a-vis ferroelectric order.<sup>27</sup> In fact, all these features such as large  $\theta/T_N$ , divergence between ZFC and FC magnetization data at a temperature above  $T_N$  (obtained from the Curie–Weiss analysis of the magnetization vs temperature data), nature of the dielectric anomaly around  $T_N$ , and its frequency-dependent shift, and so forth are consistent with the picture of the presence of strain-driven disorder and finer domains, as a result, in the sample. Interestingly, under a magnetic field of  $\sim 18$  kOe, the frequency-dependent shift of the dielectric anomaly decreases while sharpness increases. This perhaps indicates decrease of disorder, which can be attributed to the preferential alignment of the domains under a magnetic field. In Figure 4a, we show the magnetodielectric effect defined as  $[e'(0) - e'(H)]/e'(0)$  at  $T_N$  as a function of field ( $H$ ) across 0–18 kOe. Figure 4b shows thermal variation of magnetodielectric effect at  $\sim 18$  kOe across  $T_N$  at different frequencies. The magnetodielectric effect turns out to be  $>20\%$ , which is nearly comparable to what is observed<sup>28</sup> in the thin film of  $\text{Cr}_2\text{O}_3$  ( $\sim 32\%$ ). The influence of magnetic field on intrinsic capacitance of the film could be more clearly seen from the analysis of complex plane impedance spectra by the appropriate equivalent circuit model. The equivalent circuit analysis of the entire dielectric spectroscopy data across ac field frequency 100 Hz to 2 MHz takes care of dielectric relaxation of both domains and domain boundaries and helps in yielding the capacitances, separately,



(a)



(b)



(c)

**Figure 4.** (a) Magnetodielectric effect at  $T_N$  as a function of magnetic field at different frequencies within 10 kHz to 2 MHz; (b) temperature dependence of the magnetodielectric effect under  $\sim 18$  kOe; (c) magnetocapacitance effect obtained from determination of intrinsic sample capacitance ( $C$ ) under zero and  $\sim 18$  kOe field.

for both domains and domain boundaries. The capacitance obtained thus for the domains, therefore, reflects the intrinsic capacitance of the epitaxial thin film of CuO. In Figure 4c, we show the change in the intrinsic sample capacitance ( $C$ ) under  $\sim 18$  kOe magnetic field. This intrinsic magnetocapacitance effect offers the direct evidence of magnetoelectric coupling in the thin film of CuO. Of course, formation of nanoscale in-plane domains because of the presence of both compressive and tensile lattice strains in different regions of the film seems to be giving rise to drop in  $T_N$ . This is because of the

weakening of antiferromagnetic order in nanoscale domains and improvement in the ferromagnetic component. Such an observation has earlier been made in nanoscale CuO.<sup>29</sup>

We have further observed emergence of finite remanent ferroelectric polarization below  $T_N$ . The measurement of remanent hysteresis loop, at a particular temperature below  $T_N$ , employs a specially designed protocol involving application of a train of eight voltage pulses. This protocol is necessary for extracting the intrinsic hysteretic remanent ferroelectric polarization in systems where contribution from nonhysteretic polarization and leakage is strong.<sup>30</sup> The pulse train and other details of the measurement, especially, how this protocol extracts intrinsic hysteretic polarization accurately by eliminating all the spurious contributions, are given in the Supporting Information. Figure 5 shows the remanent hysteresis loops

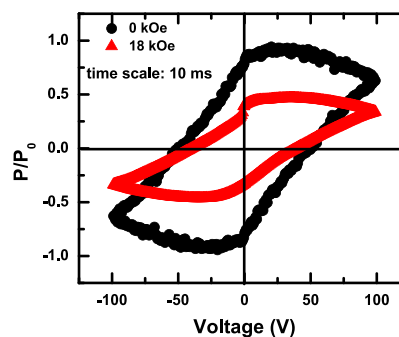


**Figure 5.** Remanent hysteresis loops measured under zero and  $\sim 18$  kOe field at  $\sim 171$  K below  $T_N$  ( $\sim 175$  K); the polarization is normalized with respect to what is observed under zero field.

measured at  $\sim 171$  K under zero and  $\sim 18$  kOe. The shape of the loop, of course, is slightly distorted. The distortion arises from (i) difference in relaxation of the nonhysteretic polarization during logic 1 and logic 0 components of the protocol (Supporting Information), (ii) influence of the finite depolarizing field at the sample-electrode interface, and (iii) difference in sample-electrode characteristics at the two electrodes used. Similar distortion of the polarization hysteresis loop has been observed by others as well.<sup>31–33</sup> Nevertheless, the presence of remanent ferroelectric polarization below  $T_N$  is evident. Comprehensive discussion of the physics behind different ferroelectric hysteresis loop shapes is available in ref 34. It is possible that alongside  $180^\circ$  domains,  $90^\circ$  domains are also involved and this, in turn, is responsible for the shape of the loop observed here. It is important to mention, in this context, that the time scale evolves, in the present case, in the counter clockwise direction along the hysteresis loop, which offers evidence in favor of the presence of intrinsic ferroelectric polarization. The loop does not arise because of charge injection. We further verify the presence of ferroelectricity in CuO by applying the PUND (positive-up-negative-down) measurement voltage pulse protocol.<sup>35</sup> PUND too yields finite hysteretic ferroelectric polarization for CuO (Supporting Information, Figure S11). Interestingly, significantly large suppression of remanent polarization by nearly 50% is observed under a magnetic field of  $\sim 18$  kOe. The large magnetodielectric effect ( $>20\%$ ) and nearly 50% suppression of remanent polarization under a magnetic field of  $\sim 18$  kOe are the central results of this paper.

It has earlier been pointed out—both from microscopic<sup>36</sup> and phenomenological<sup>37</sup> models—that cycloidal spin spiral

with propagation vector  $\vec{k}$  lying within the plane of the cycloid gives rise to ferroelectric polarization  $\vec{P}$  ( $=\vec{r} \times \vec{k}$ ). However, “proper-screw” spiral—where  $\vec{k}$  is oriented perpendicular to the plane of the cycloid—could also result in finite ferroelectricity for monoclinic or lower symmetric crystallographic structure.<sup>38</sup> The origin of ferroelectricity in the case of CuO below the magnetic transition temperature is attributed to the broken inversion symmetry via Dzyloshinskii–Moriya exchange interaction in the incommensurate spin structure comprising two magnetic sublattices.<sup>39</sup> The nonpolar  $C2/c$  structure at room temperature transforms to polar  $P2_1$  below  $T_N$  with off-centering of the Cu and O ions along  $b$ -axis. Therefore, ferroelectricity arises along crystallographic  $b$ -axis. In the cases of many such magnetic ferroelectrics, the spin flop transition under an applied magnetic field gives rise to a polarization flop as well.<sup>5</sup> Surprisingly, in the case of bulk CuO, no such transition could be observed under a moderate magnetic field. The spatially varying magnetic structure, because of its robustness resulting from large superexchange coupling parameter  $J \sim 60\text{--}80$  meV,<sup>13</sup> does not change under uniformly applied magnetic field. Therefore, no magneto-electric coupling could be observed. Application of substantially large field ( $\sim 500$  kOe) appears to be necessary in order to suppress the spiral magnetic structure and the ferroelectric polarization.<sup>14</sup> Interestingly, application of electric field is found to influence the magnetic structure in the local scale and changes the magnetic domain population.<sup>40</sup> The results obtained in the strained thin film in the present work assumes immense significance in this backdrop. The strain field generated because of large lattice mismatch couples with the ferroelectric polarization and magnetization at the *local scale*. Near degeneracy of different magnetic states<sup>41</sup> in CuO promotes such coupling as exemplified by the influence of doping<sup>42</sup> on magnetic and ferroelectric properties. This local strain field changes significantly under application of even moderate magnetic field. This, in turn, gives rise to the observed large magnetodielectric effect. A relaxed bulk sample with no locally varying strain cannot give rise to such effect under such a moderate magnetic field. The influence of coupling between strain and magnetization at the local scale could also be seen in the anomaly in resistance versus temperature plot at  $T_N$  (Figure 3a), which is conspicuously absent in bulk CuO.<sup>6</sup> It is important to point out that the strain-induced magnetoelectric coupling observed here does not result from any extrinsic effect such as domain boundaries. Evidences such as (a) emergence of finite ferroelectric polarization right below  $T_N$  ( $\sim 175$  K), (b) anomaly in resistance at  $T_N$ , and (c) large intrinsic magnetocapacitance signify strain-induced intrinsic magnetoelectric coupling in the thin film of CuO. In fact, as pointed out above, the entire dielectric spectra have been analyzed by the equivalent circuit model to separate out the domain and domain boundary effects and to yield the intrinsic bulk capacitance of the domains. It rules out the influence of domain boundaries on the observed magnetoelectric coupling. Of course, more controlled strain tuning is necessary—which ensures observation of in-plane epitaxy and prevents formation of fine domains—in order to shift the  $T_N$  toward room temperature and thereby increase the utility of the sample. It is also important to map out the evolution of the magnetoelectric properties—magnetic, ferroelectric, and their coupling—as a function of epitaxial strain by varying both the film thickness and the substrate. This will be attempted in the near future.

The present work, however, shows clearly that in the strained thin film of CuO, it is possible to observe sizable magneto-electric coupling suitable for device application.

### 3. CONCLUSIONS

In conclusion, we report that lattice strain in the epitaxial thin film of CuO deposited on the (100)MgO substrate gives rise to large magnetodielectric effect ( $>20\%$ ) and nearly 50% suppression of ferroelectric polarization under a magnetic field of  $\sim 18$  kOe. The in- and out-of-plane epitaxial strains—determined to vary within  $\pm 1\text{--}3\%$ —are instrumental in giving rise to such substantially large magnetoelectric coupling. This observation is all the more significant as strain-free bulk CuO does not exhibit such effects at such magnetic field. Controlled tuning of the strain field (either only tensile or only compressive), however, seems necessary in order to shift the magnetic transition temperature toward room temperature and tune the extent of magnetoelectric coupling. Success in such endeavor would help in projecting CuO as an alternative to BiFeO<sub>3</sub> and, hence, suitable for applications such as four-logic state memory, sensor, energy-harvesting device, spin-wave amplifier, generator, and so forth, which are based on magnetoelectric coupling.

### 4. EXPERIMENTAL SECTION

The thin films of CuO were deposited on cubic (100)MgO single-crystal substrates by pulsed laser deposition technique using KrF excimer laser ( $\lambda = 248$  nm; pulse width = 20 ns and numbers = 10,000–100,000) of energy  $\sim 3.0$  J/cm<sup>2</sup>. The results reported in this paper were obtained from the film deposited by 70,000 pulses. The base pressure of the chamber prior to deposition was  $10^{-8}$  Pa. The substrate temperature was maintained at  $\sim 560$  °C while the deposition pressure was  $\sim 20 \times 10^{-3}$  Pa. The film was finally annealed under an oxygen atmosphere during cooling ( $@5$  °C/min) for maintaining appropriate oxygen stoichiometry. In order to determine the thickness, the extent of epitaxy, the magnitude of in- and out-of-plane lattice misfit strain, and strain-driven disorder, the film was thoroughly characterized by XRD (Bruker D8 ADVANCE), TEM (model: JEOL JEM 2100 F), AFM (LT AFM/MFM; nanomagnetics), and Raman spectrometry. The dc resistivity, magnetization, dielectric, and ferroelectric properties were measured under 0–18 kOe magnetic field across 80–300 K. The electrical measurements were carried out in two-probe configuration on a sample of dimensions  $\sim 5$  mm  $\times$   $\sim 5$  mm  $\times$   $\sim 100$  nm.

### ■ ASSOCIATED CONTENT

#### Supporting Information

The Supporting Information is available free of charge at <https://pubs.acs.org/doi/10.1021/acsomega.0c02211>.

Raman spectra; AFM image with line profile data; HRTEM images showing the presence of finer “in-plane” domains; imaginary parts of the dielectric permittivity versus  $T$  plots; loss tangent data; and all the relevant details of measurement of intrinsic ferroelectric polarization (PDF)

### ■ AUTHOR INFORMATION

#### Corresponding Author

Sudipta Goswami – School of Materials Science and Nanotechnology, Jadavpur University, Kolkata 700032, India;

orcid.org/0000-0001-6331-4531;  
Email: drsudiptagoswami@gmail.com

## Authors

**Koushik Dey** – Department of Solid State Physics, Indian Association for the Cultivation of Science, Kolkata 700032, India

**Supriyo Chakraborty** – Department of Solid State Physics, Indian Association for the Cultivation of Science, Kolkata 700032, India

**Saurav Giri** – Department of Solid State Physics, Indian Association for the Cultivation of Science, Kolkata 700032, India

**Ujjal Chowdhury** – CSIR-Central Glass and Ceramic Research Institute, Kolkata 700032, India

**Dipten Bhattacharya** – CSIR-Central Glass and Ceramic Research Institute, Kolkata 700032, India; orcid.org/0000-0001-9896-1827

Complete contact information is available at:  
<https://pubs.acs.org/10.1021/acsomega.0c02211>

## Notes

The authors declare no competing financial interest.

## ACKNOWLEDGMENTS

One of the authors (S. Goswami) acknowledges support in the form of Senior Research Associateship from CSIR, Government of India, and S. Giri acknowledges support from DST (SB/S2/CMP-029/2014) Government of India. D.B. acknowledges support from CSIR (Supra Institutional Project GLASSFIB).

## REFERENCES

- Spaldin, N. A.; Ramesh, R. Advances in magnetoelectric multiferroics. *Nat. Mater.* **2019**, *18*, 203–212.
- Fiebig, M.; Lottermoser, T.; Meier, D.; Trassin, M. The evolution of multiferroics. *Nat. Rev. Mater.* **2016**, *1*, 16046.
- Catalan, G.; Scott, J. F. Physics and applications of Bismuth Ferrite. *Adv. Mater.* **2009**, *21*, 2463–2485.
- Scott, J. F. Room-temperature multiferroic magnetoelectrics. *NPG Asia Mater.* **2013**, *5*, No. e72.
- See, for example: Tokura, Y.; Seki, S.; Nagaosa, N. Multiferroics of spin origin. *Rep. Prog. Phys.* **2014**, *77*, 076501.
- Kimura, T.; Sekio, Y.; Nakamura, H.; Siegrist, T.; Ramirez, A. P. Curpice oxide as an induced-multiferroic with high- $T_C$ . *Nat. Mater.* **2008**, *7*, 291–294.
- Jones, S. P. P.; Wurz, N. C.; Failla, M.; Prabhakaran, D.; McConville, C. F.; Lloyd-Hughes, J. Influence of nonmagnetic Zn substitution on the lattice and magnetoelectric dynamical properties of the multiferroic material CuO. *Phys. Rev. B* **2014**, *90*, 064405.
- Jacobsen, H.; Gaw, S. M.; Princep, A. J.; Hamilton, E.; Toth, S.; Ewings, R. A.; Enderle, M.; Hetroy Wheeler, E. M.; Prabhakaran, D.; Boothroyd, A. T. Spin dynamics and exchange interactions in CuO measured by neutron scattering. *Phys. Rev. B* **2018**, *97*, 144401.
- Hellsvik, J.; Mentink, J. H.; Lorenzana, J. Ultrafast cooling and heating scenarios for the laser-induced phase transition in CuO. *Phys. Rev. B* **2016**, *94*, 144435.
- Rocquefelte, X.; Schwarz, K.; Blaha, P.; Kumar, S.; Brink van den, J. Room-temperature spin-spiral multiferroicity in high-pressure cupric oxide. *Nat. Commun.* **2013**, *4*, 2511.
- Jana, R.; Saha, P.; Pareek, V.; Basu, A.; Mandal, A. G.; Kapri, S.; Bhattacharya, S.; Mukherjee, G. D. High pressure experimental studies on CuO: indication of re-entrant multiferroicity at room temperature. *Sci. Rep.* **2016**, *6*, 31610.
- Kozlenko, D. P.; Druzbecki, K.; Kichanov, S. E.; Lukin, E. V.; Liermann, H.-P.; Glazyrin, K. V.; Savenko, B. N. Anomalous lattice

compression and magnetic ordering in CuO at high pressures: a structural study and first-principles calculations. *Phys. Rev. B* **2017**, *95*, 054115.

(13) Wang, F.; Zou, T.; Liu, Y.; Yan, L.-Q.; Sun, Y. Persistent multiferroicity without magnetoelectric effects in CuO. *J. Appl. Phys.* **2011**, *110*, 054106.

(14) Wang, Z.; Qureshi, N.; Yasin, S.; Mukhin, A.; Ressouche, E.; Zherlitsyn, S.; Skourski, Y.; Geshev, J.; Ivanov, V.; Gospodinov, M.; Skumryev, V. Magnetoelectric effect and phase transitions in CuO in external magnetic fields. *Nat. Commun.* **2016**, *7*, 10295.

(15) Locquet, J.-P. In-situ growth of epitaxial CuO films with a source of activated oxygen. *J. Less-Common Met.* **1990**, *164–165*, 300–306.

(16) Catana, A.; Locquet, J.-P.; Paik, S. M.; Schuller, I. K. Local epitaxial growth of CuO films of MgO. *Phys. Rev. B* **1992**, *46*, 15477–15483.

(17) Willmott, P. R.; Timm, R.; Felder, P.; Huber, J. R. Growth of CuO films by pulsed laser deposition in conjunction with a pulsed oxidation source. *J. Appl. Phys.* **1994**, *76*, 2657–2661.

(18) Kawaguchi, K.; Kita, R.; Nishiyama, M.; Morishita, T. Molecular beam epitaxy growth of CuO and Cu<sub>2</sub>O films with controlling the oxygen content by the flux ratio of Cu/O<sup>+</sup>. *J. Cryst. Growth* **1994**, *143*, 221–226.

(19) *Epitaxial growth*; Matthews, J. W., Ed.; Academic Press: New York, 1975.

(20) See, for example: Schramm, L.; Behr, G.; Löser, W.; Wetzig, K. Thermodynamic reassessment of the Cu-O phase diagram. *J. Phase Equilib. Diffus.* **2005**, *26*, 605–612.

(21) Prabhakaran, D.; Boothroyd, A. T. Single crystal growth of Zn-doped CuO by floating-zone method. *J. Cryst. Growth* **2003**, *250*, 77–82.

(22) Muthe, K. P.; Vyas, J. C.; Narang, S. N.; Aswal, D. K.; Gupta, S. K.; Bhattacharya, D.; Pinto, R.; Kothiyal, G. P.; Sabharwal, S. C. A study of the CuO phase formation during thin film deposition by molecular beam epitaxy. *Thin Solid Films* **1998**, *324*, 37–43.

(23) Seiler, W.; Millon, E.; Perrière, J.; Benzerger, R.; Boulmer-Leborgne, C. Epitaxial growth of copper oxide films by reactive cross-beam pulsed laser deposition. *J. Cryst. Growth* **2009**, *311*, 3352–3358.

(24) Hagemann, H.; Bill, H.; Sadowski, W.; Walker, E.; François, M. Raman spectra of single crystal of CuO. *Solid State Commun.* **1990**, *73*, 447–451.

(25) Wolf, I. D. Micro-Raman spectroscopy to study local mechanical stress in silicon integrated circuits. *Semicond. Sci. Technol.* **1996**, *11*, 139–154.

(26) See, for example: Feng, X.; Huang, Y.; Rosakis, A. J. On the Stoney formula for a thin film/substrate system with nonuniform substrate thickness. *Trans. ASME* **2007**, *74*, 1276–1281.

(27) Park, T.; Nussinov, Z.; Hazzard, K. R. A.; Sidorov, V. A.; Balatsky, A.; Sarrao, J. L.; Cheong, S.-W.; Hundley, M. F.; Lee, J. S.; Jia, Q. X.; Thompson, J. D. Novel dielectric anomaly in the hole-doped La<sub>2</sub>Cu<sub>1-x</sub>Li<sub>x</sub>O<sub>4</sub> and La<sub>2-x</sub>Sr<sub>x</sub>NiO<sub>4</sub> insulators: signature of an electronic glassy state. *Phys. Rev. Lett.* **2005**, *94*, 017002. ; this work shows sharp drop in dielectric permittivity around the transition in glassy system; such drop might have shown up in the form of dip following the peak in the present case signifying presence of disorder

(28) Ghosh, A.; Dey, K.; Sabyasachi, S.; Karmakar, A.; Majumdar, S.; Giri, S. Colossal magnetocapacitance near room temperature in ferromagnetic Cr<sub>2</sub>O<sub>3</sub> film. *Appl. Phys. Lett.* **2013**, *103*, 052412.

(29) Punnoose, A.; Magnone, H.; Seehra, M. S.; Bonevich, J. Bulk to nanoscale magnetism and exchange bias in CuO nanoparticles. *Phys. Rev. B* **2001**, *64*, 174420.

(30) Chowdhury, U.; Goswami, S.; Bhattacharya, D.; Midya, A.; Mandal, P. Determination of intrinsic ferroelectric polarization in lossy improper ferroelectric systems. *Appl. Phys. Lett.* **2016**, *109*, 092902.

(31) Gich, M.; Fina, I.; Morelli, A.; Sánchez, F.; Alexe, M.; Gàzquez, J.; Fontcuberta, J.; Roig, A. Multiferroic iron oxide thin films at room temperature. *Adv. Mater.* **2014**, *26*, 4645–4652.

- (32) Zheng, L.; Lin, C.; Xu, W. P.; Okuyama, M. Vertical drift of P-E hysteresis loop in asymmetric ferroelectric capacitors. *J. Appl. Phys.* **1996**, *79*, 8634–8637.
- (33) Evans, J. T. *Characterizing Ferroelectric Materials*; Radiant Technol. Inc.: New Mexico, 2011.
- (34) Scott, J. F.; Gardner, J. Ferroelectrics, multiferroics and artifacts: Lozenge-shaped hysteresis and things that go bump in the night. *Mater. Today* **2018**, *21*, 553–562.
- (35) Fina, I.; Fàbrega, L.; Langenberg, E.; Martí, X.; Sánchez, F.; Varela, M.; Fontcuberta, J. Nonferroelectric contributions to the hysteresis cycles in manganite thin films: a comparative study of measurement techniques. *J. Appl. Phys.* **2011**, *109*, 074105.
- (36) Katsura, H.; Nagosa, N.; Balatsky, A. V. Spin current and magnetoelectric effect in noncollinear magnets. *Phys. Rev. Lett.* **2005**, *95*, 057205.
- (37) Mostovoy, M. Ferroelectricity in spiral magnets. *Phys. Rev. Lett.* **2006**, *96*, 067601.
- (38) Arima, T.-h. Ferroelectricity induced by proper-screw type magnetic order. *J. Phys. Soc. Jpn.* **2007**, *76*, 073702.
- (39) Jin, G.; Cao, K.; Guo, G.-C.; He, L. Origin of ferroelectricity in high- $T_c$  magnetic ferroelectric CuO. *Phys. Rev. Lett.* **2012**, *108*, 187205.
- (40) Babkevich, P.; Poole, A.; Johnson, R. D.; Roessli, B.; Prabhakaran, D.; Boothroyd, A. T. Electric field control of chiral magnetic domains in the high temperature multiferroic CuO. *Phys. Rev. B* **2012**, *85*, 134428.
- (41) Giovannetti, G.; Kumar, S.; Stroppa, A.; van den Brink, J.; Picozzi, S.; Lorenzana, J. High- $T_c$  ferroelectricity emerging from magnetic degeneracy in cupric oxide. *Phys. Rev. Lett.* **2011**, *106*, 026401.
- (42) Hellsvik, J.; Balestieri, M.; Usui, T.; Stroppa, A.; Bergman, A.; Bergqvist, L.; Prabhakaran, D.; Eriksson, O.; Picozzi, S.; Kimura, T.; Lorenzana, J. Tuning order-by-disorder multiferroicity in CuO by doping. *Phys. Rev. B* **2014**, *90*, 014437.